Cell

Vitamin D Receptor-Mediated Stromal Reprogramming Suppresses Pancreatitis and Enhances Pancreatic Cancer Therapy

Mara H. Sherman,[1] Ruth T. Yu,[1] Dannielle D. Engle,[2] Ning Ding,[1] Annette R. Atkins,[1] Herve Tiriac,[2] Eric A. Collisson,[3] Frances Connor,[4] Terry Van Dyke,[5] Serguei Kozlov,[6] Philip Martin,[6] Tiffany W. Tseng,[1] David W. Dawson,[7] Timothy R. Donahue,[7] Atsushi Masamune,[8] Tooru Shimosegawa,[8] Minoti V. Apte,[9] Jeremy S. Wilson,[9] Beverly Ng,[10,11] Sue Lynn Lau,[10,12,13] Jenny E. Gunton,[10,11,12,13] Geoffrey M. Wahl,[1] Tony Hunter,[14] Jeffrey A. Drebin,[15] Peter J. O'Dwyer,[16] Christopher Liddle,[17] David A. Tuveson,[2] Michael Downes,[1,*] and Ronald M. Evans[1,18,*]

[1]Gene Expression Laboratory, Salk Institute, La Jolla, CA 92037, USA
[2]Cold Spring Harbor Laboratory, Cold Spring Harbor, NY 11724, USA
[3]Department of Medicine/Hematology and Oncology, University of California San Francisco, San Francisco, CA 94143, USA
[4]Cancer Research UK Cambridge Research Institute, The Li Ka Shing Centre, Robinson Way, Cambridge CB2 ORE, UK
[5]Center for Advanced Preclinical Research, NCI-Frederick, Frederick, MD 21702, USA
[6]Center for Advanced Preclinical Research, Leidos Biomed, Inc. Frederick National Laboratory for Cancer Research, Frederick, MD 21702, USA
[7]Jonsson Comprehensive Cancer Center, David Geffen School of Medicine at University of California, Los Angeles, Los Angeles, CA 90095, USA
[8]Division of Gastroenterology, Tohoku University Graduate School of Medicine, Sendai Miyagi, 980-8574, Japan
[9]Pancreatic Research Group, Faculty of Medicine, South Western Sydney Clinical School, University of New South Wales, Sydney, NSW 2052, Australia
[10]Diabetes and Transcription Factors Group, Garvan Institute of Medical Research (GIMR), Sydney, NSW 2010, Australia
[11]St Vincent's Clinical School, University of New South Wales, Sydney, NSW 2052, Australia
[12]Faculty of Medicine, University of Sydney, Sydney, NSW 2052, Australia
[13]Department of Diabetes and Endocrinology, Westmead Hospital, Sydney, NSW 2145, Australia
[14]Molecular and Cell Biology Laboratory, Salk Institute, La Jolla, CA 92037, USA
[15]Department of Surgery, Hospital of the University of Pennsylvania, Philadelphia, PA 19104, USA
[16]Abramson Cancer Center, University of Pennsylvania School of Medicine, Philadelphia, PA 19104, USA
[17]The Storr Liver Unit, Westmead Millennium Institute and University of Sydney, Westmead Hospital, Westmead, NSW 2145, Australia
[18]Howard Hughes Medical Institute, Salk Institute, La Jolla, CA 92037, USA
*Correspondence: downes@salk.edu (M.D.), evans@salk.edu (R.M.E.)
http://dx.doi.org/10.1016/j.cell.2014.08.007

SUMMARY

The poor clinical outcome in pancreatic ductal adenocarcinoma (PDA) is attributed to intrinsic chemoresistance and a growth-permissive tumor microenvironment. Conversion of quiescent to activated pancreatic stellate cells (PSCs) drives the severe stromal reaction that characterizes PDA. Here, we reveal that the vitamin D receptor (VDR) is expressed in stroma from human pancreatic tumors and that treatment with the VDR ligand calcipotriol markedly reduced markers of inflammation and fibrosis in pancreatitis and human tumor stroma. We show that VDR acts as a master transcriptional regulator of PSCs to reprise the quiescent state, resulting in induced stromal remodeling, increased intratumoral gemcitabine, reduced tumor volume, and a 57% increase in survival compared to chemotherapy alone. This work describes a molecular strategy through which transcriptional reprogramming of tumor stroma enables chemotherapeutic response and suggests vitamin D priming as an adjunct in PDA therapy.

INTRODUCTION

Cancer-associated fibroblast-like cells (CAFs) in the tumor stroma have been shown to exert a profound influence on the initiation and progression of human cancer (Bhowmick et al., 2004; Kalluri and Zeisberg, 2006; Pietras and Ostman, 2010; Räsänen and Vaheri, 2010; Shimoda et al., 2010). Pancreatic ductal adenocarcinoma (PDA) in particular is defined by a prominent stromal compartment, and numerous features ascribed to CAFs promote pancreatic cancer progression and hinder therapeutic efficacy (Mahadevan and Von Hoff, 2007). CAFs enhance PDA growth in allograft models in part via paracrine activation of pro-survival pathways in tumor cells, and inhibition of tumor-stroma interactions limits tumor progression (Hwang et al., 2008; Ijichi et al., 2011; Vonlaufen et al., 2008). Further, the dense extracellular matrix (ECM) associated with PDA obstructs intratumoral vasculature, preventing chemotherapeutic delivery (Olive et al., 2009), leading to new ideas to overcome this stromal "roadblock" (Jacobetz et al., 2013; Provenzano et al., 2012). Beyond drug delivery,

recent evidence implicates the tumor stroma in innate drug resistance in numerous tumor types (Straussman et al., 2012; Wilson et al., 2012), and treatment paradigms targeting both neoplastic cells and stromal components are emerging for PDA (Heinemann et al., 2012). While these findings suggest that CAFs in the PDA microenvironment represent a potential therapeutic target, the tumor-supporting features of pancreatic stellate cells (PSCs), the predominant fibroblastic cell type in the tumor microenvironment of the pancreas, remain poorly understood.

PSCs are nestin-positive and resident lipid-storing cells of the pancreas, with an important role in normal ECM turnover (Apte et al., 1998; Phillips et al., 2003). In health, PSCs are in a quiescent state, characterized by abundant cytoplasmic lipid droplets rich in vitamin A and low levels of ECM component production (Apte et al., 2012). During pancreatic injury, PSCs are activated by cytokines, growth factors, oxidative or metabolic stress, and transdifferentiate to a myofibroblast-like cell (Masamune and Shimosegawa, 2009). Activated PSCs lose their cytoplasmic lipid droplets, express the fibroblast activation marker α-smooth muscle actin (αSMA), acquire proliferative capacity, and synthesize abundant ECM proteins. Activated PSCs also acquire an expansive secretome which is starkly subdued in the quiescent state (Wehr et al., 2011). Persistent PSC activation under conditions of chronic injury results in pathological matrix secretion leading to fibrosis, creating a physical barrier to therapy. Further, a reciprocal supportive role for activated PSCs and pancreatic cancer cells has become increasingly appreciated: pancreatic cancer cells produce mitogenic and fibrogenic factors that promote PSC activation, such as platelet-derived growth factor (PDGF), transforming growth factor β (TGF-β), and sonic hedgehog (SHH) (Apte and Wilson, 2012; Bailey et al., 2008). Reciprocally, activated PSCs produce PDGF, insulin-like growth factor 1 (IGF1), connective tissue growth factor (CTGF), and other factors that may promote cancer cell proliferation, survival, and migration (Apte and Wilson, 2012; Feig et al., 2012). Tumor-promoting features are largely restricted to the activated PSC state; the activation process may be reversible as suggested by recent work in hepatic stellate cells (Kisseleva et al., 2012). However, the cellular factors and molecular pathways controlling this process remain elusive.

We hypothesized that pharmacologic means to revert activated cancer-associated PSCs (CAPSCs) to quiescence would hinder tumor-stroma crosstalk and tumor growth, resulting in enhanced clinical efficacy of cancer cell-directed chemotherapy. We show here that the vitamin D receptor (VDR) acts as a master genomic suppressor of the PSC activation state. VDR ligand reduces fibrosis and inflammation in a murine pancreatitis model and simultaneously undermines multiple tumor-supporting signaling pathways in PDA to enhance the efficacy of a coadministered chemotoxic agent. These results highlight a potentially widely applicable strategy to modulate stroma-associated pathologies including inflammation, fibrosis, and cancer.

RESULTS

Identification of Cancer-Associated Gene Signatures in PSCs

To characterize cancer-associated changes in PSCs, we performed massively parallel sequencing (RNA-sequencing [RNA-seq]) of the PSC transcriptome at various stages of activation. A comparison of the transcriptomes of preactivated (3-day culture) and culture-activated (7 day culture) (Omary et al., 2007) PSCs isolated from healthy mouse pancreas revealed that, during activation, PSCs decrease expression of genes implicated in lipid storage and lipid metabolism, consistent with loss of the lipid droplet phenotype associated with quiescence (Figure 1A and Figures S1A–S1C available online). Activation also resulted in increased expression of a cadre of genes with tumor-supporting potential including cytokines, growth factors, ECM components, and signaling molecules such as Wnts. Notably, cytokine induction in the stroma has been shown to promote pancreatic cancer initiation and progression in a paracrine manner (Fukuda et al., 2011; Lesina et al., 2011). In addition to the PSC "activation signature" resulting from transdifferentiation in culture, we identified a PSC "cancer signature" by comparing the transcriptomes of PSCs isolated from patients with PDA (CAPSCs) with those from patients undergoing resection for benign conditions (Figure 1B). These human PSCs were cultured (and thus culture-activated) for 15 days to achieve adequate yield and purity. This comparison of activated non-cancer-associated PSCs to cancer-associated PSCs reveals changes to the activated phenotype resulting from exposure to the tumor microenvironment. Both the activation and cancer signatures include gene classes from a previously identified stromal signature that predicts poor survival and chemoresistance in PDA (Garrido-Laguna et al., 2011). Lipid storage genes such as fatty acid binding proteins were downregulated in both signatures and were accompanied by increased expression of genes implicated in the cholesterol biosynthesis and uptake pathway, consistent with an increased proliferative capacity. Given the hypovascular nature of PDA, particularly within stromal regions, the reciprocal induction of negative angiogenic regulators and suppression of angiogenic inducers is auspicious (Figure 1C). In particular, we note the induction of thrombospondin-1 (Thbs1), a well-described and potent endogenous inhibitor of angiogenesis (Lawler, 2002). Both gene signatures include ECM components, cell adhesion molecules, inflammatory mediators, paracrine growth and survival factors, genes implicated in lipid/cholesterol metabolism, and modulators of signal transduction.

VDR Regulates the PSC Activation Network

These analyses also revealed that PSCs unexpectedly express high levels of the vitamin D receptor (VDR), previously thought not to be expressed in the exocrine pancreas (Zeitz et al., 2003) (Figures 1D, 1E, S1D, and S1E). Importantly, VDR expression is maintained in the cancer-associated PSCs (Figure 1F). We focused on this druggable receptor in light of our previous work implicating VDR as a critical regulator of the fibrogenic gene network in closely related hepatic stellate cells (Ding et al., 2013) and due to the established anti-inflammatory actions of $1,25(OH)_2D_3$ and its analogs (Cantorna et al., 1996, 1998, 2000; Ma et al., 2006; Nagpal et al., 2005). Here, we used calcipotriol (Cal), a potent and nonhypercalcemic vitamin D analog to control VDR induction (Naveh-Many and Silver, 1993). While not present in any postsurgical CAPSCs, surprisingly, Cal treatment induced lipid droplet formation in 19/27 primary patient samples

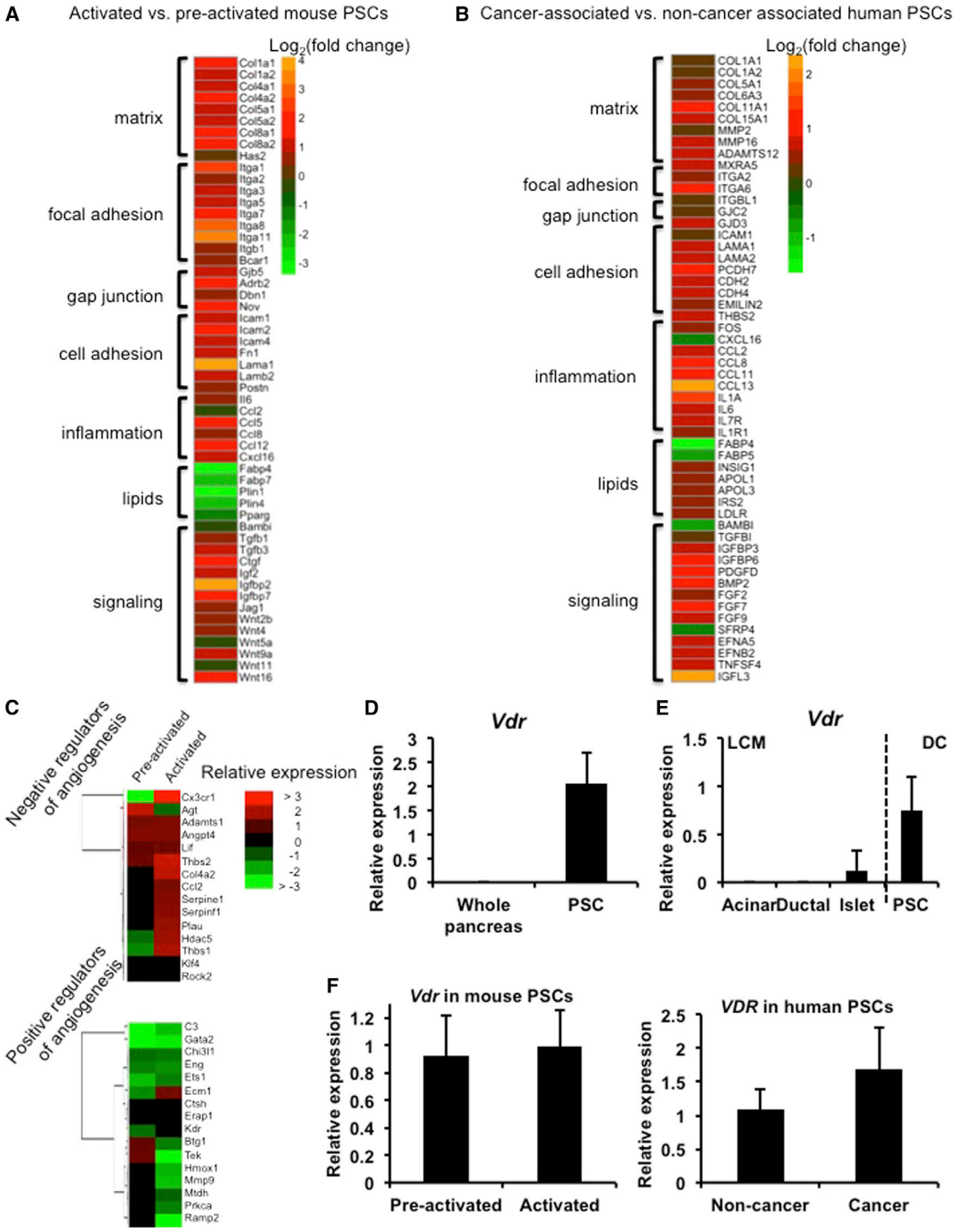

Figure 1. Activated and Cancer-Associated PSCs Exhibit a Profibrotic, Proinflammatory Phenotype

(A) Heatmap representing selected genes from RNA-seq analysis of primary mouse PSCs, demonstrating gene categories with altered expression during activation. Data are represented as $\log_2$ fold change, activated (day 7) versus preactivated (day 3), n = 3 per group.

(B) Heatmap representing selected genes from RNA-seq analysis of primary human PSCs, isolated from PDA patients (n = 5) or cancer-free donors (n = 4), and cultured for 15 days to achieve adequate yield and purity, expressed as $\log_2$ fold change PDA versus cancer-free.

(C) Heatmap showing the relative abundance of negative (top) and positive (bottom) regulators of angiogenesis in preactivated and activated primary mouse PSCs.

(D) *Vdr* expression in mouse whole-pancreas homogenates and in isolated PSCs, cultured for 3 days to expand and purify, as measured by quantitative RT-PCR (qRT-PCR).

(legend continued on next page)

(Figures 2A and S2A) and decreased expression of αSMA (*ACTA2*) in 24/27 patient samples (Figure 2B). This strongly supports the idea that the activation state is controllable in a signal-dependent fashion. To assess the genome-wide effects of VDR activation in PSCs, we performed transcriptome analysis of preactivated and activated PSCs grown in the presence or absence of VDR ligand. While Cal treatment affected gene expression in preactivated PSCs (significantly increased and decreased expression of 307 and 431 genes, respectively), VDR activation had a more widespread transcriptional response in activated PSCs (664 and 1,616 genes with significantly increased and decreased expression, respectively). Notably, we observed a Cal-dependent inhibition of the activation and cancer signatures in PSCs (Figure 2C; Table S1), including suppression of negative regulators of angiogenesis such as Thbs1 and induction of positive regulators of angiogenesis like Mmp9 (Bergers et al., 2000) (Figure 2D). Similar effects of Cal treatment were observed on selected candidate genes in human CAPSCs (Figure 2E). Furthermore, these effects were dependent on VDR, as small interfering RNA (siRNA)-mediated knockdown of the receptor abrogated Cal-induced expression changes (Figure 2F). To explain, in part, the broad impact of VDR on the PSC activation program, we assessed genomic crosstalk between VDR and the TGF-β/SMAD pathway (Schneider et al., 2001; Yanagisawa et al., 1999) that we previously demonstrated in hepatic stellate cells (Ding et al., 2013). Consistent with an inhibitory effect on TGF-β/SMAD signaling, Cal increased VDR binding while decreasing SMAD3 binding in the promoter regions of fibrogenic genes (Figures S2B and S2C). To determine whether VDR activation decreased PSC activation in vivo, we induced experimental chronic pancreatitis in wild-type mice using the cholecystokinin analog cerulein (Willemer et al., 1992) and coadministered Cal throughout disease progression. Compared to mice receiving cerulein alone, Cal-treated animals displayed attenuated inflammation and fibrosis, consistent with decreased PSC activation (Figures S3A and S3B). Expression of activation and cancer signature genes was decreased in isolated PSCs from mice treated with Cal compared to controls (Figure 3A). Reductions were observed on activation signature genes that are of functional significance in the tumor microenvironment, including ECM components, inflammatory cytokines, and growth factors. In addition, *Acta2* expression, which is associated with cell motility, trended downward. Further, reduced induction of phospho-Stat3 was observed in Cal-treated mice (Figure 3B), consistent with decreased inflammatory signaling from the stroma. Notably, Stat3 activation has been established as a mechanistic link between inflammatory damage and initiation of PDA (Fukuda et al., 2011; Lesina et al., 2011). Cal treatment during acute pancreatitis in wild-type mice similarly impaired activation-associated changes in PSC gene expression (Figure 3C) and reduced leukocyte infiltration and fibrosis (Figures 3D and 3E). Strikingly, pancreata from $Vdr^{-/-}$ mice displayed spontaneous periacinar and periductal fibrosis (Figure S3C), further supporting a role for VDR in opposing PSC activation. Consistent with this notion, activation-associated changes in PSC gene expression were augmented in cerulein-induced acute pancreatitis in $Vdr^{-/-}$ mice (Figure 3F) and were accompanied by increased fibrosis (Figure 3G). Furthermore, Cal treatment of culture-activated PSCs from $Vdr^{-/-}$ mice demonstrated the VDR dependence of the observed gene expression changes (Figure 3H). Together, these results suggest that VDR acts as a master genomic regulator of the PSC activation program, and VDR induction by ligand promotes the quiescent PSC state both in vitro and in vivo.

Stromal VDR Activation Inhibits Tumor-Supportive Signaling Events

We next assessed the impact of VDR activation in PSCs on crosstalk to tumor cells. While CAPSCs consistently expressed VDR and responded to ligand, pancreatic cancer cell lines displayed varying VDR expression and typically low VDR activity (Figures S4A and S4B). This was observed in human PDA samples as well (Figure S4C). To assess the contribution of stromal VDR activation on the epithelial compartment, we examined the effects of CAPSC-derived secreted factors on the MIAPaCa-2 cell line, which has extremely low VDR expression and no significant response to VDR ligand (Figures S4A and S4B). Primary CAPSCs were grown to confluency and cultured in the presence or absence of Cal for the final 48 hr of culture. CAPSC-conditioned media (CM) collected from these cultures was transferred to MIAPaCa-2 cells for 48 hr. Volcano plot analysis of gene expression in MIAPaCa-2 cells incubated in CAPSC CM revealed broad changes (center panel), which were largely abrogated (right panel) when CM from Cal-treated CAPSCs was used (Figure 4A). CAPSC CM induced gene expression changes in epithelial cells implicated in proliferation (Table S2), survival, epithelial-mesenchymal transition, and chemoresistance. These changes were broadly inhibited by stromal, but not epithelial, VDR activation (Figure 4B), though direct antiproliferative and proapoptotic effects of VDR activation in pancreatic cancer cells have been reported in other experimental systems (Persons et al., 2010; Yu et al., 2010). Importantly, this sensitivity to stromal, but not epithelial, VDR activation was replicated in pancreatic cancer cell lines with variable VDR expression (Figures 4C–4G). Of note, stromal VDR activation significantly reduced *CSF2* expression, implicated in pancreatic tumor progression and evasion of antitumor immunity (Bayne et al., 2012; Pylayeva-Gupta et al., 2012). Gene expression changes were accompanied by decreased induction of phospho-STAT3 (Figure 4H) and decreased resistance to chemotherapy in vitro (Figure 4I). These results demonstrate that VDR activation in PSCs negatively regulates the tumor-supporting PSC secretome.

(E) *Vdr* expression in the indicated pancreatic populations by qRT-PCR (normalized to *36B4*; n = 5). Acini, ducts, and islets were isolated by laser capture microdissection (LCM); PSCs were isolated by density centrifugation (DC).

(F) *Vdr* expression in preactivated and activated mouse PSCs (left) and in human non-cancer-associated and cancer-associated PSCs (right) determined by qRT-PCR (normalized to *36b4*, n = 3). Bars indicate the mean; error bars indicate SD.

See also Figure S1.

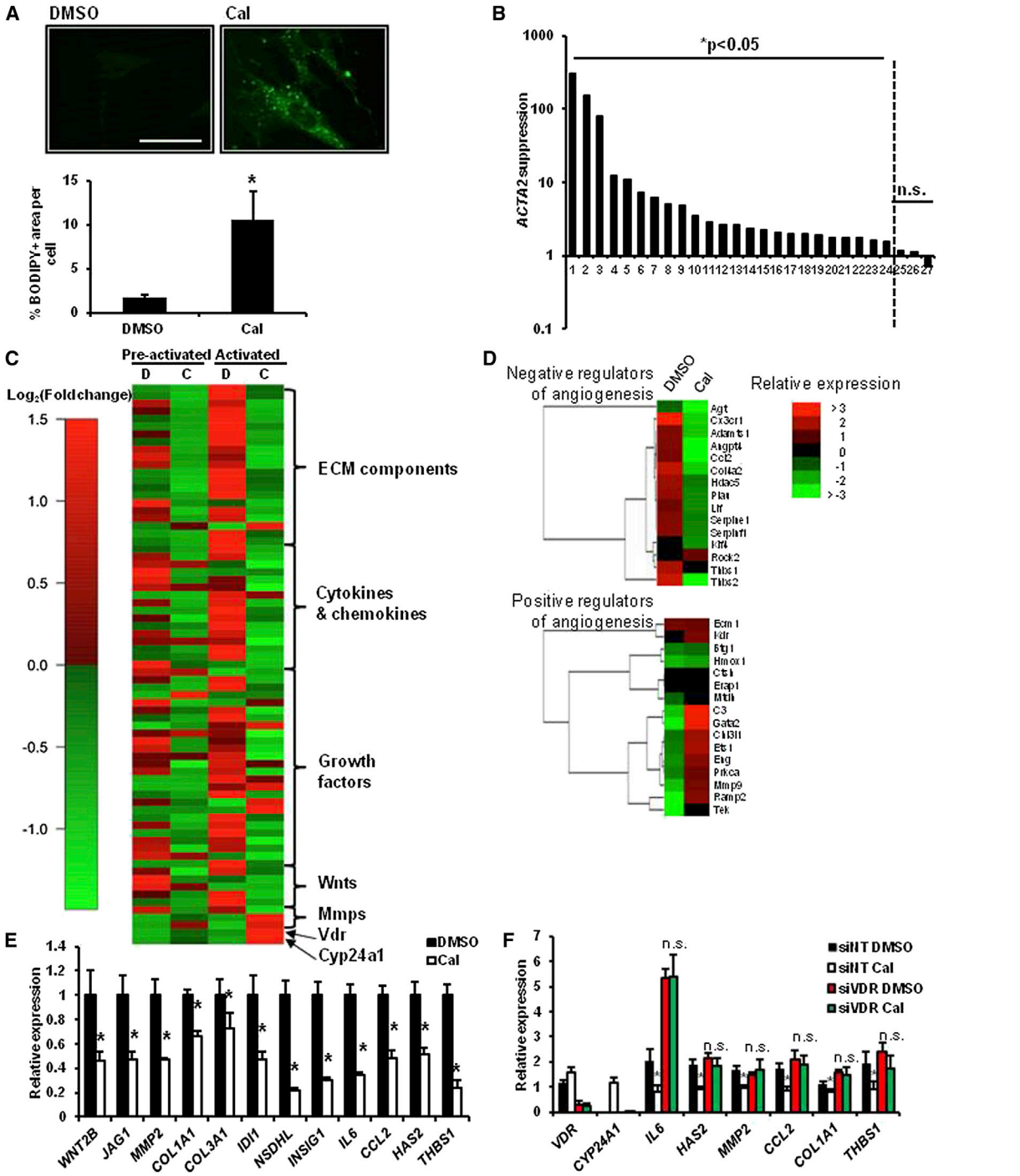

Figure 2. A VDR-Regulated Transcriptional Network Opposes PSC Activation

(A) Representative images of primary human CAPSCs treated with vehicle (DMSO) or 100 nM calcipotriol (Cal) for 48 hr and stained with BODIPY 493/503 for detection of neutral lipids. Quantification of percent BODIPY-positive area per cell in three patient samples treated with DMSO or Cal appears below, plotted as the mean + SD. Statistical significance determined by Student's unpaired t test (*$p < 0.05$). Scale bar represents 20 μm.

(B) Expression of *ACTA2* in 27 primary human CAPSCs treated with vehicle or 100 nM Cal for 48 hr. Values were plotted as DMSO/Cal and normalized to *36B4*.

(C and D) Heatmap representing selected genes from RNA-seq analysis of primary mouse PSCs treated with DMSO (D) or Cal (C) and harvested on day 3 (preactivated) or day 7 (activated) of culture after isolation (n = 3). VDR target genes *Cyp24a1* and *Vdr* are shown as controls. See also Table S1. (D) Heatmap showing the relative abundance of negative (top) and positive (bottom) regulators of angiogenesis in activated primary mouse PSCs cultured in the presence of vehicle (DMSO) or Cal.

(legend continued on next page)

VDR Ligand plus Gemcitabine Shows Efficacy against PDA In Vivo

A principal goal for PSC-targeted therapy is to exploit the inhibition of tumor-stroma crosstalk to enhance efficacy of a cytotoxic (or immunologic) agent, which in the case of gemcitabine, although standard of care, offers minimal (1.5 month) benefit to PDA patients (Burris et al., 1997). To explore the potential of vitamin D combination therapy we first explored Cal treatment in an orthotopic allograft model utilizing immune-competent hosts (Collisson et al., 2012). The tumor cells for transplantation were derived from *p48-Cre; Kras$^{LSL\text{-}G12D/+}$; p53$^{lox/+}$* mice (Bardeesy et al., 2006) and express low levels of Vdr (Figures S5A and S5B). Two other mouse PDA-derived cell lines demonstrated low VDR expression and activity as well (Figures S5A and S5B). This suggests that any observed therapeutic effect would likely result from host-derived stromal VDR activation, though some contribution from the epithelial compartment is not excluded. Although the stromal reaction in transplant models of PDA is subdued compared to the spontaneous KPC (*Kras$^{LSL\text{-}G12D/+}$;Trp53$^{LSL\text{-}R172H/+}$;Pdx-1-Cre*) model (Hingorani et al., 2005; Olive et al., 2009), measurable PSC activation of *Col1a1*, *Col1a2*, and *Acta2* was observed in allograft recipients, accompanied by fibrosis (Figures S5C and S5D). Cal treatment decreased stromal activation and fibrosis in transplanted mice (Figure S5E). Although transplant models are responsive to gemcitabine, we also compared mice treated with gemcitabine to those treated with a combination of gemcitabine and Cal. Importantly, in combination therapy recipients, we observed a clear improvement in gemcitabine responsiveness with respect to inhibition of proliferation and expression of stromal and epithelial genes from our signatures for PSC activation (Figures S5F and S5G).

We next tested the efficacy of gemcitabine plus Cal combination therapy in the KPC model, which recapitulates human PDA in poor uptake of and response to gemcitabine (Olive et al., 2009). Combination therapy significantly reduced tumor volume with transient or sustained reduced tumor growth observed in ~70% of mice (Figures 5A and S6A). In agreement with the induction of stromal remodeling, reduced tumor-associated fibrosis was observed in mice that received combination therapy compared to controls (Figure 5B). Further, combination-treated mice demonstrated significantly altered expression of genes from our stromal and epithelial gene signatures associated with PSC activation (Figure 5C). The decreased expression of PSC activation genes and induction of quiescence marker *Fabp4* suggests that the tumor-associated PSCs are shifting from an activated toward a quiescent state. The observed differential sensitivity of individual genes to the drug treatment regimens may be the result of specific perturbations to stromal-tumor paracrine signaling in vivo.

Combination therapy also increased intratumoral concentration and efficacy of gemcitabine (Figures 5D and S6B), with ~500% increase in the median concentration of dFdCTP, an active metabolite of gemcitabine, in mice that received combination therapy compared to gemcitabine alone. No drug-induced changes were seen in the expression levels of the gemcitabine degrading enzyme cytidine deaminase (Cda), the rate-limiting deoxycytidine kinase (dCK), or the nucleoside transporter Ent1 (Figure 6A), though allosteric effects are possible. Increased dFdCTP was accompanied by increased positivity for apoptotic marker CC3, indicating improved chemotherapeutic efficacy (Figure 5E). Furthermore, intratumoral vasculature was significantly increased by combination therapy, evidenced by increased CD31 positivity and apparent vessel patency (Figures 6B and 6C). While the combination of Cal with gemcitabine markedly improved therapeutic efficacy, in the absence of gemcitabine, Cal alone showed no measurable beneficial effects (data not shown). Importantly, gemcitabine plus Cal combination therapy significantly prolonged survival of KPC mice compared to chemotherapy alone, with median survival increased by 57% (median survival: Gem = 14 days, Gem + Cal = 22 days) (Figure 6D). In addition, in the Cal + Gem arm only, 29% of the mice were "long term" survivors (>30 days) with an average survival of 52.8 days.

DISCUSSION

Despite numerous attempts, the 5 year survival rate (6%) for pancreatic cancer has not changed in decades (Rahib et al., 2014). In part, this is because treatments targeting tumor cells have largely failed. The emerging role for tumor stroma as the "fuel supply-line" for cancer offers an opportunity to redirect the singular focus on the cancer cell itself to the greater tumor microenvironment (Figure 7). Indeed, by targeting VDR to transcriptionally reprogram the stroma, we simultaneously suppress inflammatory cytokines and growth factors, enhance angiogenesis, increase the efficacy of gemcitabine treatment in PDA and, most importantly, significantly improve survival.

VDR-directed therapy has a dual benefit as it reduces fibrosis and inflammation in both acute and chronic murine pancreatitis. This is significant as pancreatitis lacks any mechanistic-based therapy, is a seriously disease, and is a known risk factor for pancreatic cancer. Recently, we have shown that VDR achieves these effects by blocking TGF-β/SMAD signaling via genomic competition (Ding et al., 2013). In the acute setting, this could preclude damaging effects of an unchecked wound healing response. This balance may be tipped unfavorably by chronic tissue damage or by vitamin D deficiency, which may explain in part the inverse correlation between plasma vitamin D levels or vitamin D intake and pancreatic cancer risk (Skinner et al.,

(E) Expression levels of selected genes from the PSC activation or cancer signatures in CAPSCs treated with DMSO or 100 nM Cal for 48 hr. Results are representative of three patient samples and are plotted as the mean + SD qRT-PCR was performed in technical triplicate and values were normalized to *36B4*. Statistical significance determined by Student's unpaired t test (*$p < 0.05$).

(F) CAPSCs were transfected with siRNA pools against VDR (siVDR) or a non-nontargeting control (siNT). Cells were treated with DMSO or 100 nM Cal for 48 hr and analyzed by qRT-PCR. Values were normalized to *36B4*. Results are representative of three patient samples and are plotted as the mean + SD. Statistical significance determined by Student's unpaired t test (*$p < 0.05$; n.s. = not significant).

See also Figure S2.

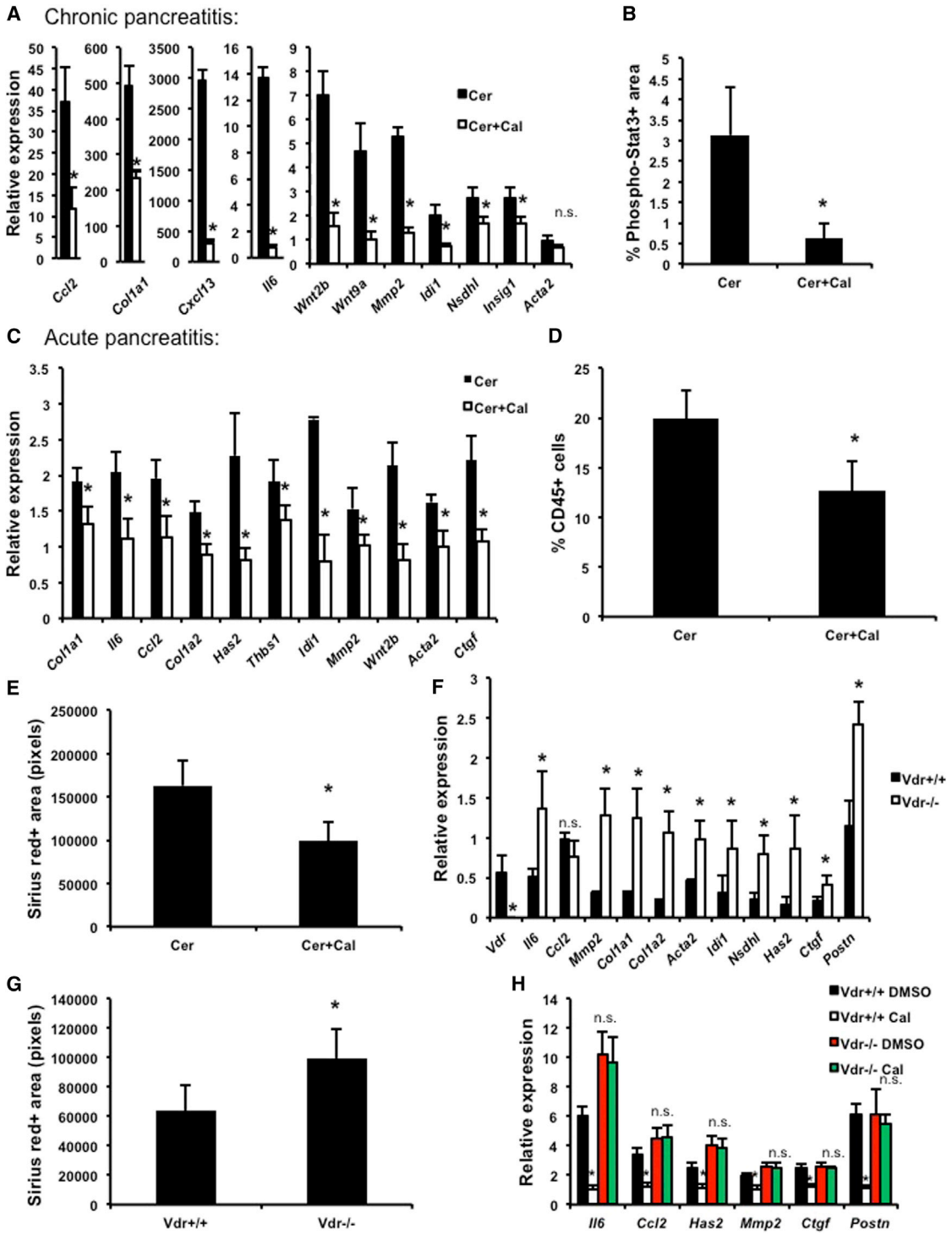

Figure 3. VDR Ligand Modulates PSC Activation In Vivo

(A) Expression levels of selected genes in PSCs isolated from mice injected with cerulein (Cer) or cerulein + Cal for 12 weeks (n = 10). Values were normalized to *36b4* and are plotted as the mean + SD.

(B) Quantification of immunofluorescent staining for phospho-Stat3 (p-Stat3) on frozen sections from wild-type mice treated with cerulein or cerulein + Cal for 12 weeks (n = 5).

(C) Expression levels of selected genes in PSCs isolated from mice injected with Cer or Cer + Cal to induce acute pancreatitis (for details see Extended Experimental Procedures; n = 5). Values were normalized to *36b4* and are plotted as the mean + SD.

(legend continued on next page)

2006; Wolpin et al., 2012) and the link between vitamin D deficiency and chronic pancreatitis (Mann et al., 2003).

Our work illustrates that transcriptional remodeling of pancreatic tumor stroma via VDR activation broadly weakens the capacity of PSCs to support tumor growth. VDR genomic targets of importance in PDA include the extracellular matrix (Jacobetz et al., 2013; Provenzano et al., 2012), the Shh pathway (Olive et al., 2009), cytokines/chemokines such as IL6 (Fukuda et al., 2011; Ijichi et al., 2011; Lesina et al., 2011), growth factors such as CTGF (Aikawa et al., 2006; Neesse et al., 2013) and Cxcl12, a mediator of the T cell blockade (Ding et al., 2013; Feig et al., 2012). This gains significance in light of recent work demonstrating that inhibition of stroma-derived survival factor CTGF potentiates the antitumor response to gemcitabine (Neesse et al., 2013) and that CXCL12 inhibition can restore T cell response. Notably, important differences exist between stromal ablation and stromal remodeling therapeutic strategies. The notion that cellular and structural components of a "normal" microenvironment exert tumor-suppressive forces and signals has been discussed previously (Bissell and Hines, 2011), although this has not been demonstrated in the pancreas and leaves in question the potential benefits of reprogrammed stroma. As VDR ligand pushes activated PSCs toward a more quiescent phenotype, it is conceivable that remodeled PSCs re-establish a physiologic and metabolic environment adverse to tumor growth, a benefit not achievable by stromal ablation. The role of VDR in tissue vitality and resilience is supported by the fact that absence of VDR in normal stroma is sufficient to promote tissue fibrosis and a hyperinflammatory response. This potential benefit of VDR-mediated stromal remodeling, to restore normal stroma, offers a conceptual advantage over stromal depletion that could leave a tissue without a critical control mechanism.

PDA stroma is believed to limit chemotherapeutic efficacy by blocking drug delivery, a result of severe hypovascularity attributable in part to dense extracellular matrix. VDR ligand significantly reduced the fibrotic content of the tumor and increased intratumoral vasculature. We also demonstrate here that activated PSCs express antiangiogenic factors such as thrombospondin-1, known to contribute to the hypovascularity in other contexts (Kazerounian et al., 2008). The antiangiogenic subset of PSC activation signature genes was suppressed by VDR ligand in vitro and, importantly, combination therapy induced improvement of tumor vascularity and drug delivery in vivo. Matrix degradation strategies that increase intratumoral blood flow and gemcitabine delivery have been shown to improve survival in PDA (Jacobetz et al., 2013; Provenzano et al., 2012). However, the significance of VDR-mediated stromal remodeling and improved vascularity with respect to long-term tumor growth and metastatic potential are currently under investigation. Indeed, the recent failure of clinical trials exploring the therapeutic potential of Shh pathway inhibition in combination with gemcitabine in pancreatic cancer bring to light potential limitations of stromal depletion therapy in the context of current treatment strategies (Amakye et al., 2013). Conceptually, reprogramming the tumor stroma and increasing functional vasculature could create a window for therapeutic delivery as well as heighten the potential for dissemination of tumor cells through the bloodstream. While activated stroma is generally considered to enhance tumor growth, two recent papers suggest that eliminating stroma by targeted deletion results in undifferentiated, aggressive pancreatic cancer and conclude that activated stroma is beneficial not harmful (Rhim et al., 2014; Ozdemir et al., 2014). Our work is not inconsistent with these studies as quiescent, vitamin A and lipid droplet-positive stromal cells are a hallmark of healthy tissue and stromal depletion strategies run the risk of eliminating key stromal components needed for tissue homeostasis. As we show, addition of Calcipotriol to gemcitabine treatment enhances survival of KPC mice by 58% while also generating significant (29%) long term survivors. Thus, in contrast to stromal depletion, we advocate that stromal reprogramming not only reduces the fuel supply line for the tumor, but it also restores normal function while allowing for enhanced chemotherapeutic efficacy and potential T cell response. Thus, in our view, coupling signal-dependent stromal reprogramming with tumor-directed cytotoxic and immunologic drugs should be the goal of new PDA therapies.

EXPERIMENTAL PROCEDURES

Cell Lines

The human pancreatic cancer cell lines MIAPaCa-2 (CRL-1420), BxPC-3 (CRL-1687), HPAC (CRL-2119), Panc1 (CRL-1469), and AsPC1 (CRL-1682) were acquired from ATCC and cultured according to supplier's instructions. The mouse pancreatic cancer cell lines p53 2.1.1, p53 4.4, and Ink 2.2 were derived from PDA in *Kras*$^{LSL\text{-}G12D/+}$; *Trp53*$^{lox/+}$; *p48-Cre* mice or *Kras*$^{LSL\text{-}G12D/+}$; *Ink4a/Arf*$^{lox/lox}$; *p48-Cre* mice (Bardeesy et al., 2006; Collisson et al., 2011) and cultured as described previously (Collisson et al., 2011, 2012). The spontaneously immortalized human pancreatic stellate cell line hPSC was isolated and established from a pancreatic cancer patient after surgical resection, as previously described (Mantoni et al., 2011). Primary PSC isolation from resected human PDA was performed in accordance with the Instutitional Review Boards of the Salk Institute for Biological Studies and the University of Pennsylvania. Description of primary PSC isolation and culture can be found in the Extended Experimental Procedures.

Animals

Kras$^{LSL\text{-}G12D/+}$;*Trp53*$^{LSL\text{-}R172H/+}$;*Pdx-1-Cre* (KPC) mice were described previously (Hingorani et al., 2005) as were *Vdr*$^{-/-}$ mice (Yoshizawa et al., 1997).

(D) Leukocyte recruitment, as measured by CD45-positive cells, in mice with acute pancreatitis (immunofluorescent staining of frozen sections, positive cells in 20× field, n = 5).

(E) Fibrosis, as measured by Sirius red staining, in mice with acute pancreatitis (per 20× field, n = 5).

(F) Expression levels of selected genes in PSCs isolated from *Vdr*$^{+/+}$ and *Vdr*$^{-/-}$ mice injected with cerulein to induce acute pancreatitis (n = 5). Means + SD are shown; values normalized to *B2M*.

(G) Sirius red-positive area in *Vdr*$^{+/+}$ and *Vdr*$^{-/-}$ mice with acute pancreatitis (per 20× field, n = 5). Statistical significance determined by Student's unpaired t test (*$p < 0.05$).

(H) Expression levels of selected genes in PSCs isolated from *Vdr*$^{+/+}$ and *Vdr*$^{-/-}$ mice after treatment with DMSO or 100 nM Cal for 48 hr. Statistical significance determined by Student's unpaired t test (*$p < 0.05$; n.s. = not significant).

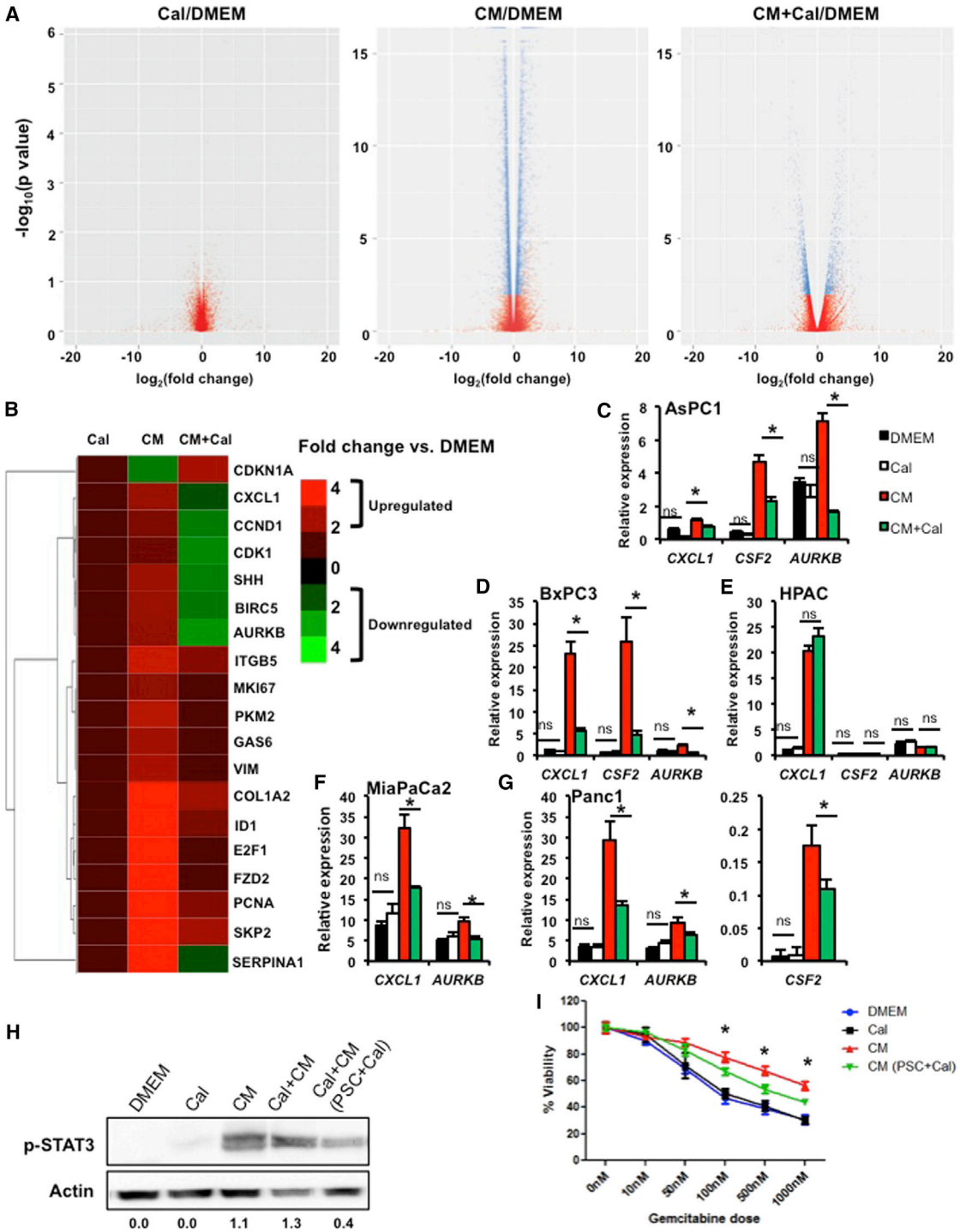

Figure 4. Stromal VDR Activation Decreases Protumorigenic Paracrine Signaling

(A) Volcano plots representing gene expression changes detected by RNA-Seq in MIAPaCa-2 cells treated with 100 nM Cal for 48 hr versus media alone (left), with CAPSC-conditioned media (CM) for 48h versus media alone (middle), or with CM from Cal-treated CAPSC (100nM, 48h) for 48h versus media alone. Blue indicates significant change; red indicates no significant change.

(B) Heatmap representing selected genes from the RNA-Seq analyses described in (A), plotted as fold change versus media alone (DMEM).

(C–G) The indicated cell lines were incubated with Cal directly, or with CM from CAPSC with or without Cal treatment, as described above. Expression levels of candidate genes *CXCL1*, *CSF2*, and *AURKB* were determined by qRT-PCR. Values were normalized to *36B4*; means + SD are shown. Statistical significance

(legend continued on next page)

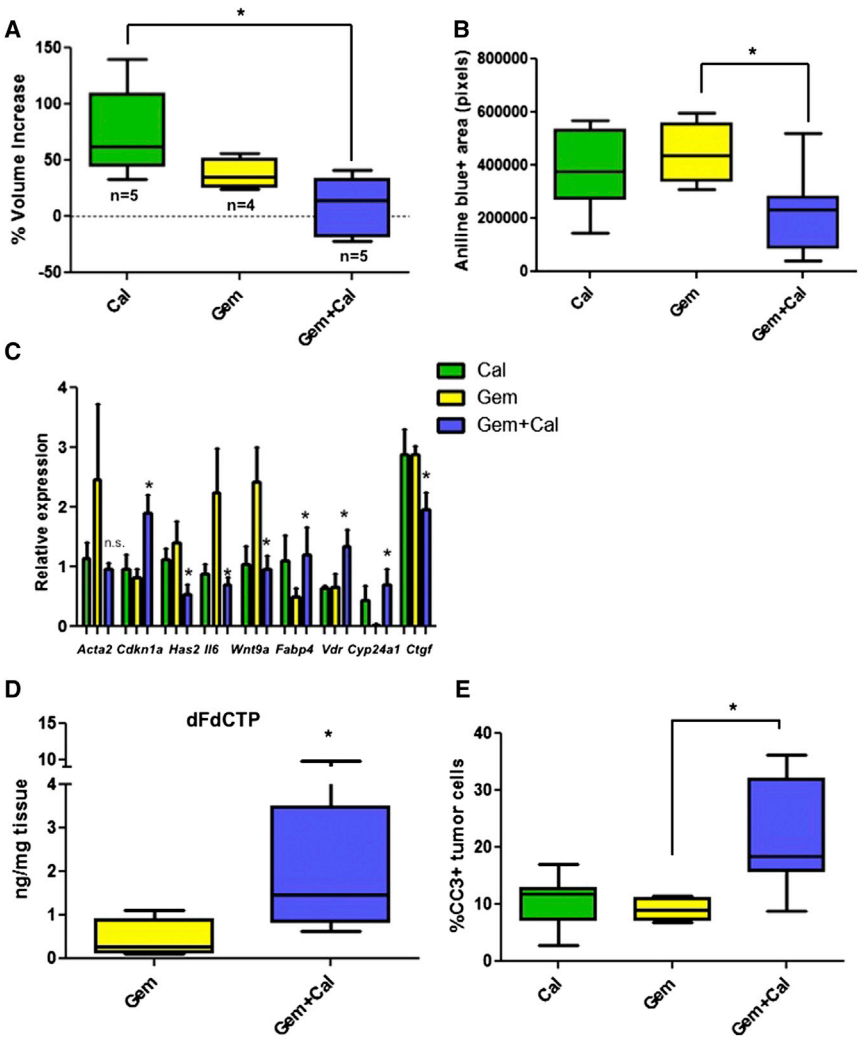

Figure 5. Stromal VDR Activation Shows Efficacy against Pancreatic Carcinoma In Vivo when Combined with Gemcitabine

KPC mice were treated for 9 days with gemcitabine (Gem), calcipotriol (Cal), or Gem + Cal (Gem: n = 4; Cal: n = 7; Gem + Cal: n = 7 unless otherwise indicated).

(A) Percent change in tumor volume at study endpoint, measured by high-resolution ultrasound. Plots indicate range, median, and quartiles. *p < 0.02; Kruskal-Wallis and Dunn's nonparametric comparison test.

(B) Aniline blue-stained collagen fibers were quantified as positive pixels per 20× field. Plots indicate range, median, and quartiles. *p < 0.05 by Mann-Whitney U test.

(C) Gene expression in tumor homogenates was determined by qRT-PCR. Values were normalized to *36b4*. Bars indicate mean + SD. *p < 0.05 by Student's unpaired t test (compared to Gem alone).

(D) Intratumoral concentrations of gemcitabine triphosphate (dFdCTP, measured by LC-MS/MS) in Gem- and Gem + Cal-treated mice 2 hr after the final dose of gemcitabine (n = 4 and 7, respectively). Plots indicate range, median, and quartiles. *p < 0.05 by Mann-Whitney U test.

(E) IHC for cleaved caspase-3 (CC3) was quantified as %CC3-positive tumor cells per 20× field. Plots indicate range, median, and quartiles. *p < 0.05 by Mann-Whitney U test.

See also Figure S4.

All animal protocols were reviewed and approved by the Institute of Animal Care and Use Committee (IACUC) of their respective institutes, and studies were conducted in compliance with institutional and national guidelines.

RNA-Seq

Total RNA (human, biological quadruplicates; mouse biological triplicates) was isolated using Trizol (Invitrogen) and the RNeasy mini kit with on-column DNase digestion (QIAGEN). For transcriptome studies, PSCs were treated with vehicle (DMSO) or 100 nM calcipotriol (Tocris) and harvested at the indicated time points. Sequencing libraries were prepared from 100–500 ng total RNA using the TruSeq RNA Sample Preparation Kit v2 (Illumina). Further details can be found in the Extended Experimental Procedures. Validation was performed by quantitative RT-PCR as described in Extended Experimental Procedures, with primer sequences provided in Table S3.

Lipid Droplet Accumulation Assay

Primary human CAPSCs, allowed to attach to glass coverslips overnight, were treated with vehicle (DMSO) or 100 nM calcipotriol for 48 hr. Washed cells were fixed (10% buffered formalin at room temperature for 15 min), then stained with 1 μg/ml 4,4-difluoro-1,3,5,7,8-pentamethyl-4-bora-3a,4a-diaza-s-indacene (BODIPY 493/503, Molecular Probes) for 1 hr at room temperature, protected from light. Washed, stained cells were mounted using Vectastain mounting media (Vector Labs) and fluorescence-visualized through the GFP filter on a Leica DM5000B microscope and quantified using ImageJ.

Conditioned Media Experiments

Primary CAPSCs were grown to 100% confluency. Fresh media was added to the cultures, and at this time, CAPSCs were treated with 100 nM calcipotriol. After 48 hr, conditioned media was harvested, sterile-filtered through 0.45 μm pores, and added to pancreatic cancer cells (PCCs) at 50%–60% confluency.

determined by Student's unpaired t test (*p < 0.05). Results are shown as replicates with one patient sample and are representative of results from multiple patient samples (n = 4), though sample-to-sample variability was noted.

(H) Immunoblot for p-STAT3 from MIAPaCa-2 cells treated for 24 hr with 100 nM Cal, CAPSC CM, Cal + CAPSC CM, or Cal + CAPSC (Cal-treated) CM. Actin served as a loading control. Values indicate densitometric ratios (p-STAT3/Actin).

(I) Viability of MIAPaCa-2 cells, treated as described above, incubated with the indicated doses of gemcitabine for 48 hr. Results are representative of three CAPSC CM samples and are plotted as the mean ± SD. Statistical significance determined by Student's unpaired t test (*p < 0.05). Asterisks designate statistically significant differences in viability between CM and CM (PSC + Cal) samples at the indicated dose of gemcitabine.

See also Figure S3 and Table S2.

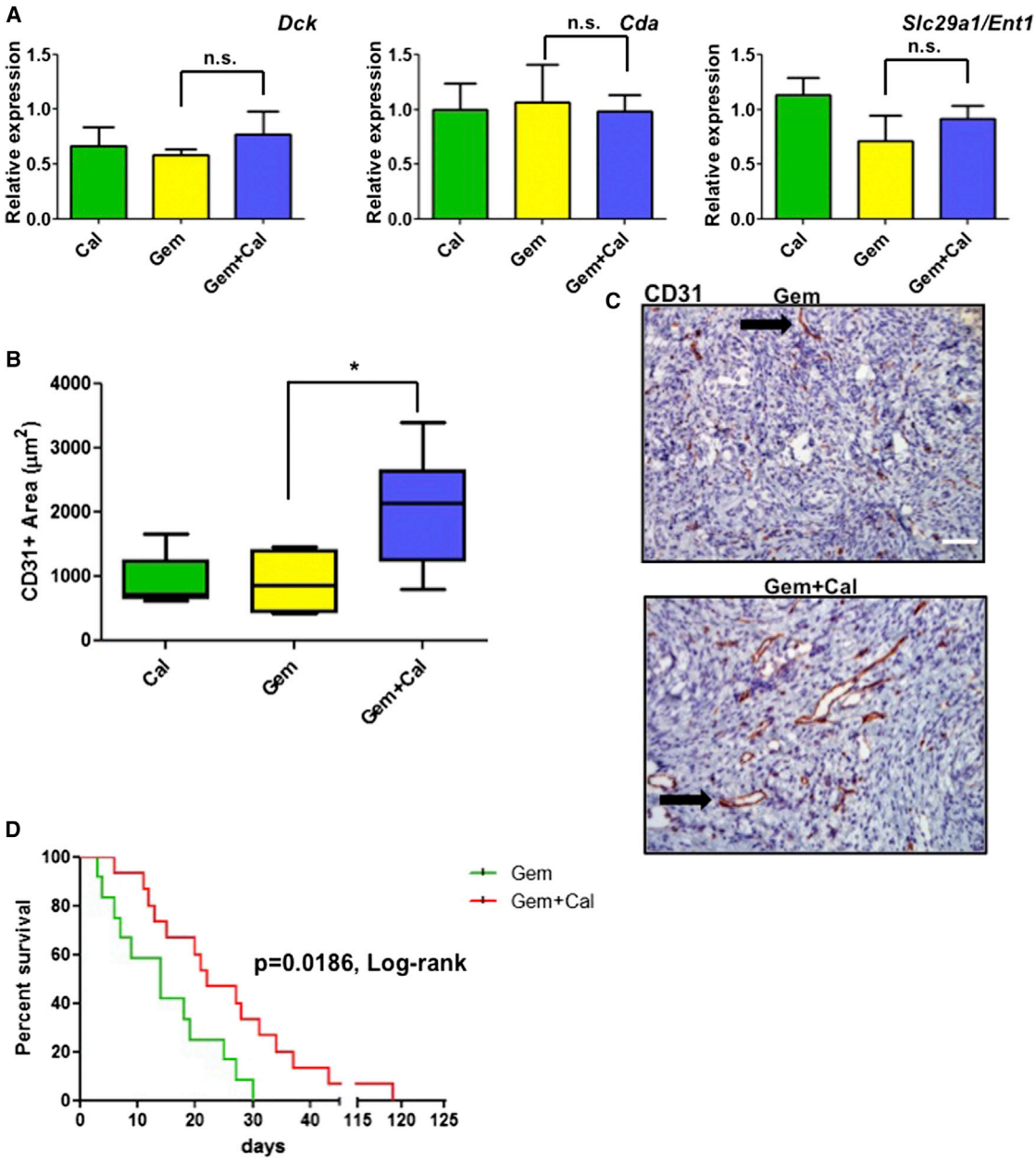

Figure 6. VDR Ligand Enhances Delivery and Efficacy of Gemcitabine

KPC mice were treated for 9 days with gemcitabine (Gem), calcipotriol (Cal), or Gem + Cal (Gem: n = 4; Cal: n = 7; Gem + Cal: n = 7 unless otherwise indicated), or treated with Gem (n = 12) or Gem + Cal (n = 15) until moribund.

(A) *Dck*, *Cda*, and *Slc29a1/Ent1* gene expression in tumor homogenates determined by qRT-PCR. Values were normalized to *36b4*. Bars indicate mean + SD.

(B) IHC for CD31 was quantified as CD31 (NovaRed)-positive area per 40× field. Plots indicate range, median, and quartiles. *$p < 0.05$ by Mann-Whitney U test.

(C) Representative CD31 IHC from Gem- and Gem + Cal-treated KPC tumors. Arrows indicate a collapsed vessel in a gemcitabine-treated tumor (top), and a vessel with an apparent lumen in a Gem + Cal-treated tumor (bottom). Scale bar represents 50 μm.

(D) Kaplan-Meier survival analysis for KPC mice treated with Gem or Gem + Cal. $p = 0.0186$ by Mantel-Cox (log rank) test.

See also Figures S5 and S6.

PCCs were treated directly with 100 nM calcipotriol at the onset of conditioned media incubation. After 48 hr, PCCs were harvested and RNA and protein isolated for analysis. For STAT3 phosphorylation experiments, MIAPaCa-2 cells were serum starved for 12 hr prior to incubation in serum-free DMEM or serum-free CM for 24 hr before cell lysis.

Orthotopic Transplant/Allograft Model

The orthotopic transplant model used here was described previously (Collisson et al., 2012). Briefly, 1×10^3 p53 2.1.1 cells were orthotopically injected into 6- to 8-week-old FVB/n mice in 50% Matrigel. After bioluminescent imaging on day 7, mice were randomized into one of four treatment groups: saline,

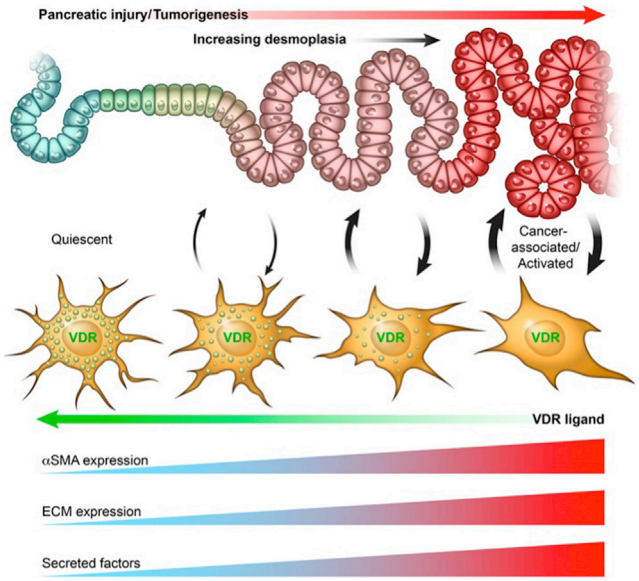

Figure 7. Model Depicting a Role for VDR in Signal-Dependent Stromal Remodeling, Limiting Pancreatic Tumor-Stroma Crosstalk

PSCs progressively acquire tumor-supporting functions during activation, a process that is driven by pancreatic injury and tumor progression via secreted factors from the epithelial compartment (and possibly from immune/inflammatory cells). VDR activation drives reversion of PSCs to a more quiescent, less tumor-supportive state. As such, cotreatment of pancreatic tumors with gemcitabine to target the tumor cells and VDR ligand to deactivate PSCs leads to an overall decrease in the reciprocal tumor-stroma crosstalk that presents a major barrier to the delivery and efficacy of gemcitabine alone.

calcipotriol (60 μg/kg intraperitoneal [i.p.], QDX20), gemcitabine (20 mg/kg i.p., Q3DX4), or calcipotriol + gemcitabine. For combination-treated mice, calcipotriol treatment began on day 7 and gemcitabine treatment began on day 14. Mice were euthanized on day 26 or when distressed, and pancreata were harvested, sliced, and flash frozen in liquid nitrogen or immediately fixed in formalin.

KPC Study Design

KPC mice with pancreatic ductal adenocarcinoma were enrolled in the study based on tumor size, as described previously (Olive et al., 2009). For the experiments in Figures 5 and 6, enrollment was restricted to mice with tumors of a mean diameter between 6 and 9 mm, as determined by high resolution ultrasound imaging. Suitable mice were assigned to a treatment group: gemcitabine, calcipotriol, or gemcitabine and calcipotriol combination. Gemcitabine was administered as a saline solution at 100 mg/kg by intraperitoneal injection, once every 3 days; when appropriate, a final dose was given 2 hr prior to euthanasia. Calcipotriol was administered as a saline solution daily at 60 μg/kg by intraperitoneal injection. Cal was administered daily for the 9 day regimen and administered every 3 days (injected with gemcitabine) for the survival study. Mice were euthanized after 9 days of treatment or at the onset of clinical signs such as abdominal ascites, severe cachexia, significant weight loss, or inactivity. Tumors were imaged by high resolution ultrasound up to twice during the 9 day treatment study.

Imaging and Quantification of KPC Tumors

High resolution ultrasound imaging of mouse pancreas was carried out using a Vevo 770 system with a 35 MHz RMV scanhead (Visual Sonics) as described previously (Dowell and Tofts, 2007). Serial 3D images were collected at 0.25 mm intervals. Tumors were outlined on each 2D image and reconstructed to measure the 3D volume using the integrated Vevo 770 software package.

Quantification of Intratumoral dFdC, dFdU, and dFdCTP by Liquid Chromatography-Tandem Mass Spectrometry

Liquid chromatography-tandem mass spectrometry (LC-MS/MS) was performed as described by Bapiro et al. (2011). Further details can be found in the Extended Experimental Procedures.

ACCESSION NUMBERS

The Gene Expression Omnibus accession number for the RNA-Seq data is GSE43770.

SUPPLEMENTAL INFORMATION

Supplemental Information includes Extended Experimental Procedures, six figures, and three tables and can be found with this article online at http://dx.doi.org/10.1016/j.cell.2014.08.007.

ACKNOWLEDGMENTS

We thank E. Ong and C. Brondos for administrative support; M. Baran, T. Guerin, J. Schlomer, J. Kalen, L. Riffel, P. Mackin, S. Kaufman, J. Alvarez, and H. Juguilon for technical assistance; and D. von Hoff and T. Bapiro for discussion. We thank T. Guerin and J. Schlomer for efficacy studies done at the Center for Advanced Preclinical Research (CAPR), the Center for Cancer Research, the National Cancer Institute. M.H.S. was supported by a Ruth L. Kirchstein National Research Service Award (T32-CA009370). This work was funded by grants from the NIH (HL105278, DK0577978, DK090962, CA014195, and ES010337), the Helmsley Charitable Trust, and the Samuel Waxman Cancer Research Foundation. R.M.E. and M.D. are supported in part by a Stand Up to Cancer Dream Team Translational Cancer Research Grant, a Program of the Entertainment Industry Foundation (SU2C-AACR-DT0509). C.L. and M.D. are funded by grants from the National Health and Medical Research Council of Australia Project Grants 512354, 632886 and 1043199. M.A. and J.W. are funded by grants from the Cancer Council of NSW. A.M. is supported by Grant-in-Aid from Japan Society for the Promotion of Science (23591008). R.M.E. is an investigator of the Howard Hughes Medical Institute and March of Dimes Chair in Molecular and Developmental Biology at the Salk Institute and supported by a grant from The Lustgarten Foundation.

Received: March 5, 2013
Revised: July 1, 2014
Accepted: July 31, 2014
Published: September 25, 2014

REFERENCES

Aikawa, T., Gunn, J., Spong, S.M., Klaus, S.J., and Korc, M. (2006). Connective tissue growth factor-specific antibody attenuates tumor growth, metastasis, and angiogenesis in an orthotopic mouse model of pancreatic cancer. Mol. Cancer Ther. *5*, 1108–1116.

Amakye, D., Jagani, Z., and Dorsch, M. (2013). Unraveling the therapeutic potential of the Hedgehog pathway in cancer. Nat. Med. *19*, 1410–1422.

Apte, M.V., and Wilson, J.S. (2012). Dangerous liaisons: pancreatic stellate cells and pancreatic cancer cells. J. Gastroenterol. Hepatol. *27* (*Suppl 2*), 69–74.

Apte, M.V., Haber, P.S., Applegate, T.L., Norton, I.D., McCaughan, G.W., Korsten, M.A., Pirola, R.C., and Wilson, J.S. (1998). Periacinar stellate shaped cells in rat pancreas: identification, isolation, and culture. Gut *43*, 128–133.

Apte, M.V., Pirola, R.C., and Wilson, J.S. (2012). Pancreatic stellate cells: a starring role in normal and diseased pancreas. Front Physiol *3*, 344.

Bailey, J.M., Swanson, B.J., Hamada, T., Eggers, J.P., Singh, P.K., Caffery, T., Ouellette, M.M., and Hollingsworth, M.A. (2008). Sonic hedgehog promotes desmoplasia in pancreatic cancer. Clin. Cancer Res. *14*, 5995–6004.

Bapiro, T.E., Richards, F.M., Goldgraben, M.A., Olive, K.P., Madhu, B., Frese, K.K., Cook, N., Jacobetz, M.A., Smith, D.M., Tuveson, D.A., et al. (2011).

A novel method for quantification of gemcitabine and its metabolites 2′,2′-difluorodeoxyuridine and gemcitabine triphosphate in tumour tissue by LC-MS/MS: comparison with (19)F NMR spectroscopy. Cancer Chemother. Pharmacol. *68*, 1243–1253.

Bardeesy, N., Aguirre, A.J., Chu, G.C., Cheng, K.H., Lopez, L.V., Hezel, A.F., Feng, B., Brennan, C., Weissleder, R., Mahmood, U., et al. (2006). Both p16(Ink4a) and the p19(Arf)-p53 pathway constrain progression of pancreatic adenocarcinoma in the mouse. Proc. Natl. Acad. Sci. USA *103*, 5947–5952.

Bayne, L.J., Beatty, G.L., Jhala, N., Clark, C.E., Rhim, A.D., Stanger, B.Z., and Vonderheide, R.H. (2012). Tumor-derived granulocyte-macrophage colony-stimulating factor regulates myeloid inflammation and T cell immunity in pancreatic cancer. Cancer Cell *21*, 822–835.

Bergers, G., Brekken, R., McMahon, G., Vu, T.H., Itoh, T., Tamaki, K., Tanzawa, K., Thorpe, P., Itohara, S., Werb, Z., and Hanahan, D. (2000). Matrix metalloproteinase-9 triggers the angiogenic switch during carcinogenesis. Nat. Cell Biol. *2*, 737–744.

Bhowmick, N.A., Neilson, E.G., and Moses, H.L. (2004). Stromal fibroblasts in cancer initiation and progression. Nature *432*, 332–337.

Bissell, M.J., and Hines, W.C. (2011). Why don't we get more cancer? A proposed role of the microenvironment in restraining cancer progression. Nat. Med. *17*, 320–329.

Burris, H.A., 3rd, Moore, M.J., Andersen, J., Green, M.R., Rothenberg, M.L., Modiano, M.R., Cripps, M.C., Portenoy, R.K., Storniolo, A.M., Tarassoff, P., et al. (1997). Improvements in survival and clinical benefit with gemcitabine as first-line therapy for patients with advanced pancreas cancer: a randomized trial. J. Clin. Oncol. *15*, 2403–2413.

Cantorna, M.T., Hayes, C.E., and DeLuca, H.F. (1996). 1,25-Dihydroxyvitamin D3 reversibly blocks the progression of relapsing encephalomyelitis, a model of multiple sclerosis. Proc. Natl. Acad. Sci. USA *93*, 7861–7864.

Cantorna, M.T., Hayes, C.E., and DeLuca, H.F. (1998). 1,25-Dihydroxycholecalciferol inhibits the progression of arthritis in murine models of human arthritis. J. Nutr. *128*, 68–72.

Cantorna, M.T., Munsick, C., Bemiss, C., and Mahon, B.D. (2000). 1,25-Dihydroxycholecalciferol prevents and ameliorates symptoms of experimental murine inflammatory bowel disease. J. Nutr. *130*, 2648–2652.

Collisson, E.A., Sadanandam, A., Olson, P., Gibb, W.J., Truitt, M., Gu, S., Cooc, J., Weinkle, J., Kim, G.E., Jakkula, L., et al. (2011). Subtypes of pancreatic ductal adenocarcinoma and their differing responses to therapy. Nat. Med. *17*, 500–503.

Collisson, E.A., Trejo, C.L., Silva, J.M., Gu, S., Korkola, J.E., Heiser, L.M., Charles, R.P., Rabinovich, B.A., Hann, B., Dankort, D., et al. (2012). A central role for RAF→MEK→ERK signaling in the genesis of pancreatic ductal adenocarcinoma. Cancer Discov *2*, 685–693.

Ding, N., Yu, R.T., Subramaniam, N., Sherman, M.H., Wilson, C., Rao, R., Leblanc, M., Coulter, S., He, M., Scott, C., et al. (2013). A vitamin D receptor/SMAD genomic circuit gates hepatic fibrotic response. Cell *153*, 601–613.

Dowell, N.G., and Tofts, P.S. (2007). Fast, accurate, and precise mapping of the RF field in vivo using the 180 degrees signal null. Magn. Reson. Med. *58*, 622–630.

Feig, C., Gopinathan, A., Neesse, A., Chan, D.S., Cook, N., and Tuveson, D.A. (2012). The pancreas cancer microenvironment. Clin. Cancer Res. *18*, 4266–4276.

Fukuda, A., Wang, S.C., Morris, J.P., 4th, Folias, A.E., Liou, A., Kim, G.E., Akira, S., Boucher, K.M., Firpo, M.A., Mulvihill, S.J., and Hebrok, M. (2011). Stat3 and MMP7 contribute to pancreatic ductal adenocarcinoma initiation and progression. Cancer Cell *19*, 441–455.

Garrido-Laguna, I., Uson, M., Rajeshkumar, N.V., Tan, A.C., de Oliveira, E., Karikari, C., Villaroel, M.C., Salomon, A., Taylor, G., Sharma, R., et al. (2011). Tumor engraftment in nude mice and enrichment in stroma- related gene pathways predict poor survival and resistance to gemcitabine in patients with pancreatic cancer. Clin. Cancer Res. *17*, 5793–5800.

Heinemann, V., Haas, M., and Boeck, S. (2012). Systemic treatment of advanced pancreatic cancer. Cancer Treat. Rev. *38*, 843–853.

Hingorani, S.R., Wang, L., Multani, A.S., Combs, C., Deramaudt, T.B., Hruban, R.H., Rustgi, A.K., Chang, S., and Tuveson, D.A. (2005). Trp53R172H and KrasG12D cooperate to promote chromosomal instability and widely metastatic pancreatic ductal adenocarcinoma in mice. Cancer Cell *7*, 469–483.

Hwang, R.F., Moore, T., Arumugam, T., Ramachandran, V., Amos, K.D., Rivera, A., Ji, B., Evans, D.B., and Logsdon, C.D. (2008). Cancer-associated stromal fibroblasts promote pancreatic tumor progression. Cancer Res. *68*, 918–926.

Ijichi, H., Chytil, A., Gorska, A.E., Aakre, M.E., Bierie, B., Tada, M., Mohri, D., Miyabayashi, K., Asaoka, Y., Maeda, S., et al. (2011). Inhibiting Cxcr2 disrupts tumor-stromal interactions and improves survival in a mouse model of pancreatic ductal adenocarcinoma. J. Clin. Invest. *121*, 4106–4117.

Jacobetz, M.A., Chan, D.S., Neesse, A., Bapiro, T.E., Cook, N., Frese, K.K., Feig, C., Nakagawa, T., Caldwell, M.E., Zecchini, H.I., et al. (2013). Hyaluronan impairs vascular function and drug delivery in a mouse model of pancreatic cancer. Gut *62*, 112–120.

Kalluri, R., and Zeisberg, M. (2006). Fibroblasts in cancer. Nat. Rev. Cancer *6*, 392–401.

Kazerounian, S., Yee, K.O., and Lawler, J. (2008). Thrombospondins in cancer. Cell. Mol. Life Sci. *65*, 700–712.

Kisseleva, T., Cong, M., Paik, Y., Scholten, D., Jiang, C., Benner, C., Iwaisako, K., Moore-Morris, T., Scott, B., Tsukamoto, H., et al. (2012). Myofibroblasts revert to an inactive phenotype during regression of liver fibrosis. Proc. Natl. Acad. Sci. USA *109*, 9448–9453.

Lawler, J. (2002). Thrombospondin-1 as an endogenous inhibitor of angiogenesis and tumor growth. J. Cell. Mol. Med. *6*, 1–12.

Lesina, M., Kurkowski, M.U., Ludes, K., Rose-John, S., Treiber, M., Klöppel, G., Yoshimura, A., Reindl, W., Sipos, B., Akira, S., et al. (2011). Stat3/Socs3 activation by IL-6 transsignaling promotes progression of pancreatic intraepithelial neoplasia and development of pancreatic cancer. Cancer Cell *19*, 456–469.

Ma, Y., Khalifa, B., Yee, Y.K., Lu, J., Memezawa, A., Savkur, R.S., Yamamoto, Y., Chintalacharuvu, S.R., Yamaoka, K., Stayrook, K.R., et al. (2006). Identification and characterization of noncalcemic, tissue-selective, nonsecosteroidal vitamin D receptor modulators. J. Clin. Invest. *116*, 892–904.

Mahadevan, D., and Von Hoff, D.D. (2007). Tumor-stroma interactions in pancreatic ductal adenocarcinoma. Mol. Cancer Ther. *6*, 1186–1197.

Mann, S.T., Stracke, H., Lange, U., Klor, H.U., and Teichmann, J. (2003). Vitamin D3 in patients with various grades of chronic pancreatitis, according to morphological and functional criteria of the pancreas. Dig. Dis. Sci. *48*, 533–538.

Mantoni, T.S., Lunardi, S., Al-Assar, O., Masamune, A., and Brunner, T.B. (2011). Pancreatic stellate cells radioprotect pancreatic cancer cells through β1-integrin signaling. Cancer Res. *71*, 3453–3458.

Masamune, A., and Shimosegawa, T. (2009). Signal transduction in pancreatic stellate cells. J. Gastroenterol. *44*, 249–260.

Nagpal, S., Na, S., and Rathnachalam, R. (2005). Noncalcemic actions of vitamin D receptor ligands. Endocr. Rev. *26*, 662–687.

Naveh-Many, T., and Silver, J. (1993). Effects of calcitriol, 22-oxacalcitriol, and calcipotriol on serum calcium and parathyroid hormone gene expression. Endocrinology *133*, 2724–2728.

Neesse, A., Frese, K.K., Bapiro, T.E., Nakagawa, T., Sternlicht, M.D., Seeley, T.W., Pilarsky, C., Jodrell, D.I., Spong, S.M., and Tuveson, D.A. (2013). CTGF antagonism with mAb FG-3019 enhances chemotherapy response without increasing drug delivery in murine ductal pancreas cancer. Proc. Natl. Acad. Sci. USA. Published online July, 2013. http://dx.doi.org/10.1073/pnas.1300415110.

Olive, K.P., Jacobetz, M.A., Davidson, C.J., Gopinathan, A., McIntyre, D., Honess, D., Madhu, B., Goldgraben, M.A., Caldwell, M.E., Allard, D., et al. (2009). Inhibition of Hedgehog signaling enhances delivery of chemotherapy in a mouse model of pancreatic cancer. Science *324*, 1457–1461.

Omary, M.B., Lugea, A., Lowe, A.W., and Pandol, S.J. (2007). The pancreatic stellate cell: a star on the rise in pancreatic diseases. J. Clin. Invest. *117*, 50–59.

Ozdemir, B.C., Pentcheva-Hoang, T., Carstens, J.L., Zheng, X., Wu, C.C., Simpson, T.R., Laklai, H., Sugimoto, H., Kahlert, C., Novitskiy, S.V., et al. (2014). Depletion of carcinoma-associated fibroblasts and fibrosis induces immunosuppression and accelerates pancreas cancer with reduced survival. Cancer Cell *25*, 719–734.

Persons, K.S., Eddy, V.J., Chadid, S., Deoliveira, R., Saha, A.K., and Ray, R. (2010). Anti-growth effect of 1,25-dihydroxyvitamin D3-3-bromoacetate alone or in combination with 5-amino-imidazole-4-carboxamide-1-beta-4-ribofuranoside in pancreatic cancer cells. Anticancer Res. *30*, 1875–1880.

Phillips, P.A., McCarroll, J.A., Park, S., Wu, M.J., Pirola, R., Korsten, M., Wilson, J.S., and Apte, M.V. (2003). Rat pancreatic stellate cells secrete matrix metalloproteinases: implications for extracellular matrix turnover. Gut *52*, 275–282.

Pietras, K., and Ostman, A. (2010). Hallmarks of cancer: interactions with the tumor stroma. Exp. Cell Res. *316*, 1324–1331.

Provenzano, P.P., Cuevas, C., Chang, A.E., Goel, V.K., Von Hoff, D.D., and Hingorani, S.R. (2012). Enzymatic targeting of the stroma ablates physical barriers to treatment of pancreatic ductal adenocarcinoma. Cancer Cell *21*, 418–429.

Pylayeva-Gupta, Y., Lee, K.E., Hajdu, C.H., Miller, G., and Bar-Sagi, D. (2012). Oncogenic Kras-induced GM-CSF production promotes the development of pancreatic neoplasia. Cancer Cell *21*, 836–847.

Rahib, L., Smith, B.D., Aizenberg, R., Rosenzweig, A.B., Fleshman, J.M., and Matrisian, L.M. (2014). Projecting cancer incidence and deaths to 2030: the unexpected burden of thyroid, liver, and pancreas cancers in the United States. Cancer Res. *74*, 2913–2921.

Räsänen, K., and Vaheri, A. (2010). Activation of fibroblasts in cancer stroma. Exp. Cell Res. *316*, 2713–2722.

Rhim, A.D., Oberstein, P.E., Thomas, D.H., Mirek, E.T., Palermo, C.F., Sastra, S.A., Dekleva, E.N., Saunders, T., Becerra, C.P., Tattersall, I.W., et al. (2014). Stromal elements act to restrain, rather than support, pancreatic ductal adenocarcinoma. Cancer Cell *25*, 725–737.

Schneider, E., Schmid-Kotsas, A., Zhao, J., Weidenbach, H., Schmid, R.M., Menke, A., Adler, G., Waltenberger, J., Grünert, A., and Bachem, M.G. (2001). Identification of mediators stimulating proliferation and matrix synthesis of rat pancreatic stellate cells. Am. J. Physiol. Cell Physiol. *281*, C532–C543.

Shimoda, M., Mellody, K.T., and Orimo, A. (2010). Carcinoma-associated fibroblasts are a rate-limiting determinant for tumour progression. Semin. Cell Dev. Biol. *21*, 19–25.

Skinner, H.G., Michaud, D.S., Giovannucci, E., Willett, W.C., Colditz, G.A., and Fuchs, C.S. (2006). Vitamin D intake and the risk for pancreatic cancer in two cohort studies. Cancer Epidemiol. Biomarkers Prev. *15*, 1688–1695.

Straussman, R., Morikawa, T., Shee, K., Barzily-Rokni, M., Qian, Z.R., Du, J., Davis, A., Mongare, M.M., Gould, J., Frederick, D.T., et al. (2012). Tumour micro-environment elicits innate resistance to RAF inhibitors through HGF secretion. Nature *487*, 500–504.

Vonlaufen, A., Joshi, S., Qu, C., Phillips, P.A., Xu, Z., Parker, N.R., Toi, C.S., Pirola, R.C., Wilson, J.S., Goldstein, D., and Apte, M.V. (2008). Pancreatic stellate cells: partners in crime with pancreatic cancer cells. Cancer Res. *68*, 2085–2093.

Wehr, A.Y., Furth, E.E., Sangar, V., Blair, I.A., and Yu, K.H. (2011). Analysis of the human pancreatic stellate cell secreted proteome. Pancreas *40*, 557–566.

Willemer, S., Elsässer, H.P., and Adler, G. (1992). Hormone-induced pancreatitis. Eur. Surg. Res. *24* (*Suppl 1*), 29–39.

Wilson, T.R., Fridlyand, J., Yan, Y., Penuel, E., Burton, L., Chan, E., Peng, J., Lin, E., Wang, Y., Sosman, J., et al. (2012). Widespread potential for growth-factor-driven resistance to anticancer kinase inhibitors. Nature *487*, 505–509.

Wolpin, B.M., Ng, K., Bao, Y., Kraft, P., Stampfer, M.J., Michaud, D.S., Ma, J., Buring, J.E., Sesso, H.D., Lee, I.M., et al. (2012). Plasma 25-hydroxyvitamin D and risk of pancreatic cancer. Cancer Epidemiol. Biomarkers Prev. *21*, 82–91.

Yanagisawa, J., Yanagi, Y., Masuhiro, Y., Suzawa, M., Watanabe, M., Kashiwagi, K., Toriyabe, T., Kawabata, M., Miyazono, K., and Kato, S. (1999). Convergence of transforming growth factor-beta and vitamin D signaling pathways on SMAD transcriptional coactivators. Science *283*, 1317–1321.

Yoshizawa, T., Handa, Y., Uematsu, Y., Takeda, S., Sekine, K., Yoshihara, Y., Kawakami, T., Arioka, K., Sato, H., Uchiyama, Y., et al. (1997). Mice lacking the vitamin D receptor exhibit impaired bone formation, uterine hypoplasia and growth retardation after weaning. Nat. Genet. *16*, 391–396.

Yu, W.D., Ma, Y., Flynn, G., Muindi, J.R., Kong, R.X., Trump, D.L., and Johnson, C.S. (2010). Calcitriol enhances gemcitabine anti-tumor activity in vitro and in vivo by promoting apoptosis in a human pancreatic carcinoma model system. Cell Cycle *9*, 3022–3029.

Zeitz, U., Weber, K., Soegiarto, D.W., Wolf, E., Balling, R., and Erben, R.G. (2003). Impaired insulin secretory capacity in mice lacking a functional vitamin D receptor. FASEB J. *17*, 509–511.